Efficient White-Light Visible Light Communication With Novel Optical Antennas Based on Luminescent Solar Concentrators

Marco Meucci, Sandra Doria, Ali Muhammad Umair, Daniele Franchi, Marco Fattori, Mariangela Di Donato, Alberto Picchi, Andrea Pucci, Massimo Calamante, and Jacopo Catani

***Abstract*—OpticalAntennas (OAs) based on Fluorescent Concentrators (FCs) promise a revolution in the deployment of Visible Light Communication (VLC) and Optical Wireless Communication (OWC), due to their inherent advantages over conventional receivers in terms of exceedingly larger field of view (FoV) and optical gain (OG). Whilst FC-based OAs have been demonstrated in VLC applications in a wealth of works embedding monochromatic UV and Blue LED sources, a detailed study demonstrating the performances of OA in white-light VLC (WLC) applications, which is at the basis of the deployment of VLC for Internet of Things (IoT), 6G and pervasive networks, is still lacking. In our work we present and test two 50 mm x 50 mm OAs for WLC, based on two of the most effective fluorophores (Lumogen© Red 305 F and DQ1, respectively) used in Luminescent Solar Concentrator (LSC) applications. We perform a detailed characterization of intrinsic and VLC performances, comparing the results with a novel Monte Carlo model accurately describing the photon conversion and propagation processes. Whilst DQ1 represents the most suited solution for high-speed VLC with UV/blue LEDs, our results highlight excellent performances of Lumogen-based OA in white-light settings, outpacing the performances of ordinary photodiode-based receivers. Our results pave the way towards the full-fledged deployment of VLC in IoT applications, where the availability of detectors with large-area, wide FoV and enhanced OG covering the white LEDs emission is a central element.**

***Index Terms*—Li-Fi, luminescent solar concentrators, optical antennas, visible light communication, VLC.**

Manuscript received 4 July 2023; revised 19 September 2023, 26 October 2023, and 20 November 2023; accepted 24 November 2023. Date of publication 27 November 2023; date of current version 2 April 2024. This work was supported in part by the CNR Progetti di Ricerca@CNR "FluoCom", in part by the MiSE CTE PRato Industrial SMart Accelerator "CTE-PRISMA," and in part by the European Union - NextGeneration EU, "Integrated infrastructure initiative in Photonic and Quantum Sciences" - I-PHOQS under Grants IR0000016, ID D2B8D520, and CUP B53C22001750006. *(Corresponding author: Jacopo Catani.)*

This work did not involve human subjects or animals in its research.

Marco Meucci, Ali Muhammad Umair, and Jacopo Catani are with the National Institute of Optics-CNR (CNR-INO), I-50019 Sesto Fiorentino, Italy, and also with the European Laboratory for NonLinear Spectrosopy (LENS), I-50019 Sesto Fiorentino, Italy (e-mail: marco.meucci@ino.cnr.it; umair@lens.unifi.it; jacopo.catani@ino.cnr.it).

Sandra Doria, Daniele Franchi, Mariangela Di Donato, and Massimo Calamante are with the Institute for Chemistry of Organometallic Compounds (CNR-ICCOM), I-50019 Sesto Fiorentino, Italy (e-mail: doria@lens.unifi.it; daniele.franchi@iccom.cnr.it; didonato@lens.unifi.it; mcalamante@iccom.cnr.it).

Marco Fattori is with the Physics and Astronomy Department, University of Florence, 50121 Florence, Italy, and also with the European Laboratory for NonLinear Spectrosopy (LENS), I-50019 Sesto Fiorentino, Italy (e-mail: marco.fattori@unifi.it).

Alberto Picchi and Andrea Pucci are with the Chemistry and Industrial Chemistry Department, University of Pisa, I-56124 Pisa, Italy (e-mail: alberto.picchi@phd.unipi.it; andrea.pucci@unipi.it).

Color versions of one or more figures in this article are available at https://doi.org/10.1109/JLT.2023.3337040.

Digital Object Identifier 10.1109/JLT.2023.3337040

I. Introduction

THE constantly increasing request for wireless data connections and the related congestion of radio-frequency (RF) spectrum makes it necessary to exploit other bands of the electromagnetic spectrum in order to achieve full-fledged deployment of long-sought services and architectures such as Internet of Things (IoT) [1], [2], Smart Cities [3], Intelligent Transportation Systems (ITS) [4], and Augmented Reality Services [5]. For this reason, next-generation wireless platforms such as 6G [6] will fully encompass the optical domain to wirelessly cast data over the air, relieving the issues related to RF spectrum congestion [7]. In light of this, researchers have been working on Visible Light Communication (VLC) for the past decade, aiming at exploitation of ordinary LED sources to provide for fast, reliable and pervasive wireless communications along with illumination and signaling. In VLCs, data are encoded over the optical carrier as intensity modulation, theoretically supporting extremely large bandwidths (BW), increased intrinsic security, and very low latency [8], [9] as compared to common RF-based technologies, making it a key candidate for the implementation of future communication networks [10], [11], [12], [13]. Several recent studies have been carried out embedding fast LED sources and receivers, reporting very high data rates ranging from several hundred Mbps to Gbps [14], [15], [16]. However, the majority of these pioneering studies were typically carried out in a laboratory setting [17], [18], exploiting small-sized, fast LEDs as a source, or even on micro LEDs [19], achieving relatively short communication links in a very protected environment. This approach is hardly suitable for the implementation of realistic VLC links or Li-Fi architecture [20], the latter aiming at the exploitation of ordinary high-power white LEDs (WLEDs) as illumination and communication sources. As white LEDs typically feature an intrinsically reduced BW of a few MHz [21] due to the presence of a layer of phosphors slowly converting a portion of blue light into yellow, seminal works studied the possibility to realize high-speed, white-light VLC (WLC) links by blue

filtering the light at receiver [22]. Filtering indeed eliminates the slow phosphor component and improves the overall BW of the system, with the possibility of attaining Gbps rates when advanced equalization [23], [24] and modulation [25] techniques are put in play. However, in situations where ultra-high data rates are not a priority, as in the case of most IoT applications [26], [27], this method is not ideal as it wastes a major portion of optical power available from the LED source [28], negatively impacting the attainable haul of WLC links. Furthermore, as the communication link lengthens, the large spatial divergence of common LED lamps makes it essential to have a large Optical Gain (OG) at the receiver, to maintain a high signal-to-noise ratio (SNR). In photodiode (PD)-based receiver (RX) stages, however, maintaining a large OG without a complementary reduction of the Field of View (FoV) is impossible due to the Eténdue principle [29], while the RX sensitivity cannot be increased arbitrarily by enlarging the PD size, as this intrinsically limits its BW due to parasitic capacitance effects [30]. The limitations in FoV, size and sensitivity of RX stages are even more evident in free-space optical communication (FSO) implementations, where the long-haul of the link boosts the effects of dynamical misalignment between transmitter (TX) and receiver (RX) stages due to beam wandering [31], severely affecting the communication performances and quality.

Taking such scenarios into account, an ideal RX stage for VLC must feature high OG, high BW, and relaxed misalignment sensitivity. To tackle this challenge, researchers have recently proposed a break-through approach, developing Optical Antennas (OA) based on Fluorescent Concentrators (FC) [32], [33]. FC-based OAs are thin, planar substrates, fabricated by dispersing a fluorophore into a polymeric matrix [34], [35], and capable of converting the impinging photon flux towards longer wavelengths with a given quantum yield (ϕ) [36]. Due to the high refractive index of the polymeric host, the re-emitted light is wave-guided towards the edges of the slab, which could embed a small-area, fast PD. The effective receiving area of OA can hence be made much larger than a typical PD, yet preserving large BWs and relaxed angular dependence as compared to ordinary optical condensing stages [29]. Such an approach could have a profound impact on the implementation of pervasive VLC, as FC OAs can be virtually integrated in devices like laptops, mobile phones etc. [37]. Furthermore, as FCs can relax misalignment issues and the related need for complex pointing tracking systems, their potential becomes evident also for FSO communications [38] and long-range VLC applications [39]. By properly selecting fluorophores with reduced fluorescent lifetimes, pioneering works implementing planar shaped FC OAs successfully achieved transmission at very high baud rates up to few Gbps [40]. In most cases, FCs are realized using organic fluorophores, (OFs), initially developed for different applications yet featuring suitable properties for VLC, like absorption in the visible spectrum and a high fluorescence. The most commonly used OF is Coumarin 6 [29], [33], [41], [42] as it possesses good optical properties, but it suffers from poor compatibility with the polymeric matrix and low stability [43]. Other examples of less performing OFs include BODIPY derivatives [44], characterized by a low fluorescence, and pentaphenylenes [45], which have absorption below 400 nm and thus cannot be utilized with white LEDs. Perylene diimides, such as the LR305, exhibit good stability and compatibility with PMMA, which is one of the most commonly used polymeric matrix, as well as a high fluorescence, and have been proposed for VLC applications [46], but no evidence for WLED communication has been reported yet. Recent comparative studies analyzed the time response of several FC in VLC applications [46]. Others also considered different geometries from simple planar slabs. For instance, in [47], non-planar (spherical) geometries have been realized through fluorescent flexible fibers absorbing the UV-portion of the visible spectrum (< 405 nm), as well as flexible nanostructured FCs [38] have been demonstrated, both exploiting violet LEDs as TX sources [48]. However, even if recent results highlighted limitations of UV-absorbing fluorescent fibers as RX stages in white-light VLC systems, the vast majority of works employs Blue-UV LED sources, as most reported FC-based OAs feature the largest absorption in the Blue-UV spectral region [46]. A few attempts have been made to realize FC OAs exploiting white light. Recently, a multi-layer OA has been reported, performing wavelength division multiplexing (WDM) in the blue and green regions of visible spectrum, respectively [33]. In [49] an OA design using three distinct commercially available fluorescent fibers is presented, selectively absorbing different wavelength ranges, such as to cover the spectrum of a WLED. Similarly, in [50] a simulation-based scheme for an OA integrating three distinct fluorophores is suggested, with no experimental confirmation for the proposed scheme. To fill the gap in unleashing the full potential of VLC with WLED sources, in this paper we build and test OAs exploiting two organic fluorophores (OF) originally developed and successfully employed for solar conversion, namely Lumogen Red© 305 F (LR305), the commercial benchmark for Luminescent Solar Concentrator (LSC) applications [51], [52] and DQ1, a recently synthesized quinoxaline chromophore that was reported to feature excellent optical properties in LSC. [53]. The two chromophores have different spectral properties: while DQ1 has an intense absorption peaked at 430 nm, fluorescing with high ϕ and large Stokes shift, LR305 absorbs over a large portion of the solar spectrum, with smaller Stokes shift. Comparing the performances of the two FC with WLED sources is an essential step to select the most suited OA in WLC applications.

To this scope, here, we perform a thorough experimental characterization of the two OAs, measuring their intrinsic properties (such as BW and wavelength-dependent efficiency), as well as their communication performances embedding them as OA in a complete WLC system, as a function of the link length. We corroborate our analysis with a detailed Monte Carlo model to estimate the efficiency of both FCs as a function of wavelength, accounting for geometrical propagation, multiple internal reflections and re-absorption processes, for several LED sources. The paper is structured as follows: Section II-A provides a comprehensive description and analysis of the LR305 and DQ1 fluorophores, including their absorption and emission spectra. Section III gives details on the experimental characterization of FC slabs prepared with the two fluorophores, such as rise and fall times and collection efficiency, and presents the Monte Carlo

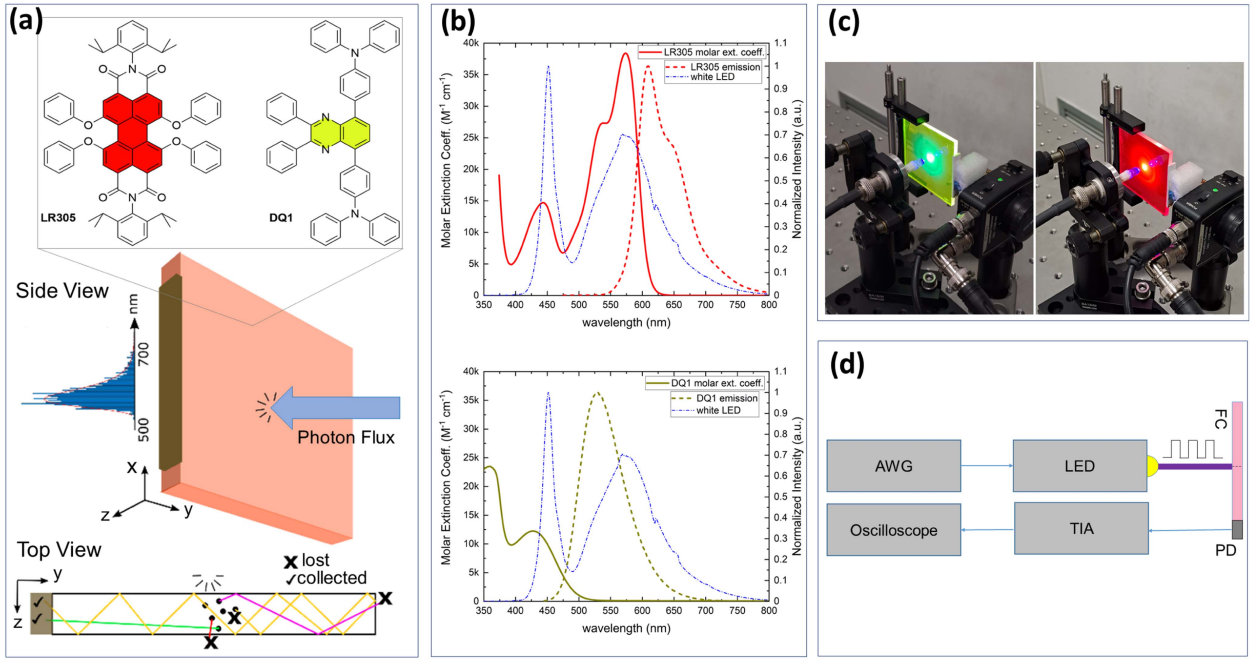

Fig. 1. (a) Top: Chemical structure of LR305 and DQ1. The perylene and quinoxaline cores are highlighted in red and green respectively. Bottom: schematic representation of the FC slab and of the internal reflection paths for converted photons; (b) absorption (solid lines) and emission (dashed lines) spectra of the two OF in the realized PMMA slabs (conc. 350 ppm); blue dashed line correspond to WLED emission spectrum; (c) image of the implemented OAs, and (d) block diagram of the experimental setup for efficiency and time-response measurement setup.

model along with its predictions. In Section IV, we describe the experimental campaign embedding both FCs as OAs in WLC configuration and recording their performances in terms of quality of VLC transmission, including achievable maximum data rate and achievable transmission distance. Finally, in Section V, we present our conclusions and summarize the obtained results.

II. Properties of Selected FCs and Realization of OAs

A. Properties of LR305 and DQ1

The chemical structure of the two employed chromophores, LR305 and DQ1, is depicted in Fig. 1(a). In our study, LR305 (Fig. 1(a)), currently considered as the best performing OF in LSC applications [54], has been chosen as a benchmark, as it features a very good overlap between its absorption band and WLED spectrum (see Fig. 1(b)), and it is easily available in the market. On the other side, like most symmetric perylene fluorophores, LR305 presents a limited Stokes shift and, given the significant overlap between its absorption and emission spectra (Fig. 1(b)), the performances of large-area FCs fabricated with this dye are generally limited because of self-absorption phenomena [55]. Limiting self-absorption is of particular importance in VLC applications, as it induces losses due to secondary re-absorption processes, and may also introduce temporal delays into light transmission to the receiver, potentially limiting the maximum achievable BW for high bit rates when large substrates are realized [46]. The other selected OF, DQ1, has the advantage of achieving Stokes shifts as large as 116 nm (0.61 eV), yet retaining easy and economic synthetic paths, with a noticeable fluorescence ϕ. Absorption and emission spectra of the FCs realized with the two fluorophores are reported in Fig. 1(b). LR305 (upper panel) features a main broad absorption band peaked at 574 nm, with a shoulder at 536 nm and a lower intensity band peaking at 443 nm, thus covering a broad region of the UV-visible spectrum. Its fluorescence is peaked at 611 nm with a Stokes shift limited to 37 nm. When compared to LR305, absorption and emission spectra of DQ1 (centered at 430 and 530 nm, respectively, see Fig. 1(b)) are blue-shifted, but the spectral overlap is reduced. Both OF present good ϕ values of 0.83 (LR305) and 0.87 (DQ1), in the realized FCs. Previous characterization demonstrated that the fluorescence lifetime of both fluorophores is approximately 8 ns, thus well suited for VLC applications with BW up to several MHz [53], [56]. The trade-off between the two OFs is not easy: whilst LR305 overlaps well with the WLED spectra, DQ1 has a higher ϕ and lower self-absorption, making it nontrivial to foresee which could perform better in WLC.

B. Realization of FC Slabs and Integration as OA

FC slabs doped with LR305 or DQ1 were realized by free radical polymerization. PMMA free radical polymerizations were performed by cell casting, pouring a solution of methyl methacrylate (TRE CI s.r.l., Teramo, Italy), poly(methyl methacrylate) powder (DIAKON, Mw = 95,000 g/mol, Lucite International), fluorophore and initiators into a $(25 \times 25 \times 0.3)$ cm mold. Molds are composed of two glass sheets separated by PVC gasket, whose thickness is adjusted to match that required for the PMMA sheet when pressed. Metallic clamps allow the mold to remain sealed during polymerization. The pouring resin

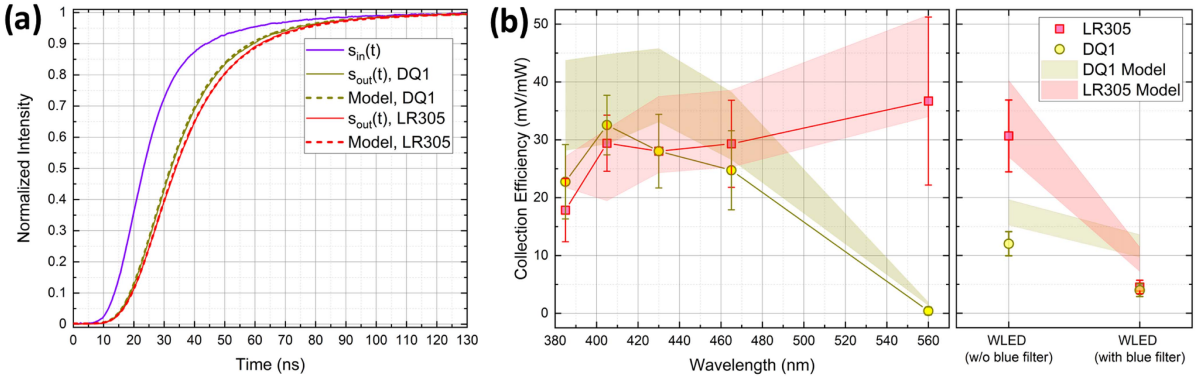

Fig. 2. (a) Rise time of LR305 and DQ1 FCs (red and dark yellow solid lines, respectively) when stimulated by a BW-limited pulse of violet light (purple line). Dashed lines represent the function obtained applying the model (see text), minimizing the deviation from $s_{out}(t)$. (b) Symbols represent the power-normalized collection efficiency of LR305 and DQ1 OAs, measured with LEDs at different wavelengths (left panel), and with white LED, with and w/o blue filter (right panel). Shaded areas represent the predictions of our Monte Carlo model, with their related uncertainty.

(300 g) contains 60 g of DIAKON (20 wt.%), 240 g of MMA (80 wt.%), and 0.30 g of Azobisisobutyronitrile (AIBN, Sigma Aldrich, USA) (0.1 wt.%), Lumogen F Red 305 (Abcr GmbH, Germany) or DQ1 (synthesized according to the literature [53]) were added in the desired concentration (350 ppm). The sealed mold was placed in a water-filled tank overnight at a temperature of 50 °C, then transferred to an oven for 4 hours, reaching 120 °C. At the end of the curing process, the two glass sheets were separated, and the PMMA slab was cut to size by laser cutting and polished, reaching a plane square geometry, with 50 mm × 50 mm × 3 mm dimensions (W × H×T). OAs are then realized by coupling one of the 50 mm × 3 mm edges of the FC slabs to a fast PD (Fig. 1(a)–(c)), collecting the fluorescence photons and converting them into electrical current. In efficiency and communication tests (Sections III-A and IV, respectively) the OAs embed a 30 mm × 3 mm Si PD (Hamamatsu S3588-09), whose photo-current is voltage-converted and amplified by a specially-made trans-impedance amplifier (TIA) with 12 MHz BW. A multi-order AC filtering stage is embedded before TIA to filter out low frequency unwanted light components below 1 KHz, and to avoid DC saturation [57]. The customized PD and TIA stage has BW of 12 MHz for minimum TIA gain (G = 0 dB). Part of the wave-guided photons will escape the slab and will not be collected by the PD, whose dimensions are slightly smaller than the edge size. This leaves space for further geometrical optimization in future versions of our OAs. Conversely, in time-response analysis (Section III-A) the custom PD+TIA stage is replaced by a commercial avalanche PD featuring 400 MHz BW (APD, Thorlabs APD430 A/M) with a reduced active area of 0.2 mm^2. In this case, indeed, we target a faster response than the OF lifetime, rather than a large collection efficiency.

III. Characterization and Modeling of Intrinsic Properties of Optical Antennas

A. Characterization of Time Response and Efficiency

To determine the frequency response of the FCs, we implement a high-BW TX stage by driving a low-power violet LED (15 mW @ 405 nm, Thorlabs LED405E) through an arbitrary waveform generator (AWG) (Siglent SDG6022X). First, by applying square current pulses on the LED, we record the optical signal $s_{in}(t)$ emitted by the LED through the APD, observing optical rise and fall times of $\sim$ 30 ns (BW = 12 MHz) (Fig. 2(a)). Then, to detect the FC response, the light source is placed in the center of the slab, almost in contact with the surface, driven by the same square wave current. The light emitted by the antenna, denoted as $s_{out}(t)$, is recorded by a 200 MHz digital oscilloscope (Tektronix, MDO3024) by positioning the APD at one of the edges of the FC (Fig. 1(c)). The observed time responses are reported as solid lines in Fig. 2(a).

As shown by [46], if the self-absorption probability is small, the time response of a FC can be described as a first-order low-pass filter. To estimate its cutoff frequency we calculate the convolution of $s_{in}(t)$ with a decaying exponential and determine the time constant that minimizes the deviation of the convoluted function from $s_{out}(t)$. The comparison between these two curves is reported in Fig. 2. The time constants estimated from the fit result $\tau_{\mathrm{LR305}} = (11.1 \pm 0.2)$ ns for LR305 slab and $\tau_{\mathrm{DQ}} = (9.52 \pm 0.12)$ ns for DQ1 slab. A similar analysis has been also performed on the falling edge of the signal, yielding the same values, within the experimental uncertainties. The agreement between simulation and experiment is excellent, although the measured time constants result slightly larger than the ones already reported in the literature [53], [56]. Further studies will be required to investigate the origin of this discrepancy. We plan to perform similar experiments with larger FCs slabs and with variable distances between the detector and the point where the light impinges on the OA. This will allow to model and quantify the effect of multi-photon reabsorption, that is known to increase the response time of the antennas [46]. Finally, we stress that the convolution method we adopted allows to estimate the values of the time constants with high precision even if they are smaller than the rising time of the LED signal.

In order to evaluate the wavelength-dependent efficiency of VLC receivers we exploit a setup similar to the one described above, where the APD is replaced by our custom PD+TIA stage (Section II-A). PD is placed in contact with the slab at the mid point of a lateral edge, and several monochromatic LEDs sources

are used (385 nm, 405 nm, 430 nm, 465 nm, and 560 nm), as well as a WLED (Thorlabs LEDW7E) with and without a blue filter (Thorlabs, FB450-40). Whilst LSC setups often involve external efficiency measurements, defined as the ratio of photons collected at the edges of the FC with respect to the photons impinging the OA [58], [59], we rather measure a more direct quantity, i.e. the *collection efficiency* η_{coll}, by placing each LED, driven to its nominal current value, at a fixed, short distance in front of the OAs. We then record the amplitude of the converted signal after PD+TIA stage for each source, neglecting the fluorescence photons escaping from uncovered portions of the edges. In order to present comparable efficiency results, η_{coll} is retrieved by normalizing the recorded amplitudes to the corresponding optical power of each LED, measured through a power meter (Ophir Nova PD-300, 1-cm^2 active area). The short distance between LED and OAs makes the LED emission pattern to be fully contained in the OA's surface. Fig. 2(b) reports η_{coll} as a function of wavelength (left panel). Error bars are obtained by error propagation of experimental uncertainties on PD and LED positioning, LED power, and signal amplitude. Results show that OAs realized with both DQ1 and LR305 exhibit similar performances in the UV-blue region, with a slightly larger efficiency of DQ1 at 380 nm and 405 nm as compared to LR305, associated with its stronger absorption in the blue region (see Fig. 1(b)). However, as expected from absorption spectra, the efficiency of DQ1 considerably drops as compared to LR305 for wavelengths longer than 430 nm, while LR305 features an exceedingly larger yield in the green-yellow region around 560 nm, which is an essential band for WLED-based communications. To confirm this point, right panel of Fig. 2(b) reports a similar analysis involving a WLED source, with and without blue filtering. As data show, LR305 has a nearly treble efficiency as compared to DQ1 when white light is used, while when the blue filter is inserted the global yield of both OFs decreases as a consequence of the lower optical power available after the filter. However, whilst LR305 features a decrease of 85% as compared to the unfiltered case, DQ1 features a lower reduction (62%), leading to similar performances with blue-filtered light. This is mainly due to the self-blue-filtering effect inherent to the absorption profile of DQ1, not absorbing the green-yellow components of WLED. Given the observed efficiencies, one could argue better overall performances when using LR305-based OA in WLC applications. However, as LR305 also retains the slow components of WLED light, a non-trivial trade-off could stem from competition between larger collection efficiency and slower response of LR305 as compared to DQ1 in WLC applications, underlining the need for direct communication tests in specific baud rate conditions (Section IV).

B. Efficiency Monte Carlo Model

The photon transport in the slabs has been simulated by implementing a Monte Carlo model developed using MATLAB programming language [60] and following previous literature on ray-tracing computational models [50], [61], [62], [63], The main input parameters of the model are the geometry of the slab, ϕ (respectively 0.83 and 0.87 for LR305 and DQ1), the experimental absorption and emission spectra of the slabs doped with the OFs, the measured power and emission spectrum of the light source. In the simulations, 10^5 photons from different LED sources are randomly generated within the emission distribution of the LED and uniformly distributed within the measured radius of 3 mm, considering the LED placed in contact with the slab surface and at its center. The experimental geometry is described in Fig. 1(a). Fresnel reflections are taken into account at the air-slab interfaces (PMMA reflectivity $= 4\%$). After entering the slab, the free path ΔS of each photon is computed using the Lambert-Beer law, considering the experimental absorption spectra (Fig. 1(b)) and the known concentration of the dye (350 ppm):

$$\Delta S = -\frac{\log(r)}{\epsilon(\lambda)M}, \tag{1}$$

where r is a random variable between [0,1], $\epsilon(\lambda)$ is the molar extinction coefficient of the dye, and M the molar concentration. Absorbed photons are isotropically re-emitted with a probability ϕ, with a wavelength distribution corresponding to the emission spectrum (Fig. 1(b)). With reference to Fig. 1(a), each photon travels within the slab until it is alternatively:

- re-absorbed after travelling a free path ΔS ((1)), and eventually re-emitted, depending on ϕ;
- lost due to transmission at a slab surface, according to the Fresnel equations for total internal reflection (TIR) for unpolarized light, considering the refractive index change at the surface (n_{slab} =1.49, n_{air}=1);
- collected from the detector, after multiple TIR reflections at the slab surfaces. Only the photons impinging the active area of the detector placed in contact with the surface (detector-to-slab distance $= 50\,\mu$m) are considered.

The present model features several improvements with respect to previously reported works. It implements angle-dependent Fresnel reflections at the OAs edges and at the detector's air-silicon interface ($\eta_{silicon} = 3.46$), and allows both the convolution of the power spectrum of the collected photons [W] with the detector spectral responsivity [A/W], and the conversion to measured voltage, accounting for TIA gain [V/W], which finally allows to obtain the collection efficiency [mV/mW] for direct comparison with the experiments.

The results of the Monte Carlo simulations for each LED source are plotted in Fig. 2(b) as shaded areas, whose extension represents the confidence interval of the simulation, determined by varying each input parameter within its experimental uncertainty interval (10% uncertainty in concentration, 5% uncertainty in ϕ, 2% uncertainty in refractive index, and a 50% uncertainty in the PD to slab distance). The residual discrepancy between model and data could be due to scattering effects occurring in the substrates, and to losses due to non-perfect optical quality of slabs, not accounted for by the model.

IV. VLC Tests With LR305 and DQ1 Optical Antennas

A. System Architecture for VLC Tests

To experimentally assess the performances of LR305 and DQ1 for WLC applications, we embed our new OAs as optical receivers (Section II-B) in a complete VLC system (See Fig. 3). We perform bit error rate (BER) measurements through

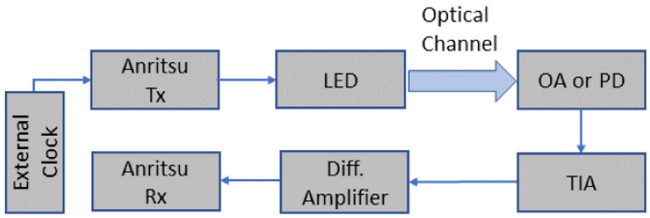

Fig. 3. Block diagram of the experimental setup for WLC communication tests and BER analysis.

a synchronous digital transmission analyzer (Anritsu ME520B BERT system), with an external clock distributed to both the TX and RX modules (Fig. 3). The data pattern is represented by a $(2^{15}-1)$ pseudo-random binary sequence (PRBS) with non-return-to-zero, on-off keying (OOK-NRZ). The VLC TX stage is realized by driving the WLED with the TX module, so that the digital PRBS sequence is replicated on the optical channel as intensity modulation on white light. For VLC RX stage, we consider two different configurations: the first [*White*] corresponds to a condition where the full white WLED spectrum impinges onto OAs, whilst the second [*Filtered*] embeds the 450-nm optical filter in front of WLED (see Section III-A). The configuration [*bare PD*] in which the PD is used as a direct RX front-end is also analyzed for reference. The PD output after OAs is band-pass filtered by means of a unitary gain amplifier (LeCroy, DA1822 A) and sent to the RX block of the BERT system, measuring data integrity and reporting the BER value. We carried out transmission tests at rates of 1 Mbps and 5 Mbps.

B. VLC Data Transmission Analysis: BER vs Amplitude/SNR

Fig. 4(a) shows the BER values measured for the experimental configurations discussed above, as a function of the peak-to-peak amplitude of the signal received at the PD output. Red (yellow) symbols correspond to data for LR305 (DQ1) OAs. Blue symbols represent [*bare PD*] cases. Error bars (not shown not to overload the figure) are obtained as the standard deviation on recorded data, and correspond to $\sim 4\%$ and ± 0.2 mV on the vertical and horizontal axis, respectively. First considering the 5 Mbps rate, the [*bare PD, White*] and [*LR305, White*] cases feature similar BER values, higher than all other cases, and in particular of the [*LR305, Filtered*] case. This is justified by the fact that at this rate the slow phosphor component of WLED lowers the overall BW, so that the overall SNR, for a given signal amplitude, is lower. Conversely, by either using blue-filtered light or the DQ1 fluorophore, slow components are not converted and the SNR is higher. This is more evident by looking at eye-diagrams, recorded for each experimental configurations for a fixed amplitude of 15 mV via a digital oscilloscope (Keysight, InfiniiVision DSOX6004 A) at 5 Mbps, and reported in Fig. 4(b). The BW-limiting effect of yellow phosphors is evident in both [*bare PD, White*] and [*LR305, White*] cases, leading to slower transitions and narrower eye widths. Interestingly, this effect is evident in neither [*Filtered*] cases, nor in the [*DQ1, White*] case, where the BW corresponds to the intrinsic BW of the blue component of WLED (~ 9.4 MHz). Considering the lower data rate of 1 Mbps, no sizeable differences in performances are observed, indicating that both LR305 and DQ1 similarly behave in WLC links because of their intrinsic lifetime (Section III-A) is lower than the WLED rise time (~ 160 ns, BW~ 2.2 MHz).

We note that cases with similar peak-to-peak amplitudes, yet featuring different signal distortion due, e.g. to different BWs, could lead to different BER values as a consequence of a different SNR value, defined as SNR $= \mathrm{S_{RMS}}/\sigma_{\mathrm{noise}}$, where $\mathrm{S_{RMS}}$ is the RMS signal amplitude after PD, and σ_{noise} is the measured RMS noise value in the decoder BW. However, by considering purely additive white Gaussian noise and binary OOK modulation, and in case no synchronization errors are considered, the BER should only depend upon SNR through $\mathrm{BER} = \frac{1}{2}\mathrm{erfc}(\mathrm{SNR})$ [64]. By calculating $\mathrm{S_{RMS}}$ and σ_{noise} we can re-plot BER data as a function of SNR (see Fig. 4(c)). The calculation is performed on the recorded tracks of amplitude values measured before the input stage of RX module. Oscilloscope tracks are BW limited to 200 MHz, which approximately matches the input BW of the RX module, so that $\mathrm{S_{RMS}}$ and σ_{noise} are effectively calculated in the decoder BW. Fig. 4(c) reports the comparison between data and the predictions of the model (shaded area) with no free parameters, taking into account a technical offset $\mathrm{S_{offs}} = 6.5\,\mathrm{mV}$ affecting the discriminator module, lowering the effective SNR by a factor $\mathrm{S_{offs}}/\sigma_{\mathrm{noise}} \simeq 9$. The BER model is calculated using the rescaled value $(\mathrm{SNR} - 9)$. The width of the area on Fig. 4(c) corresponds to a confidence interval obtained by including a 5% error in the experimental value of the offset.

Importantly, as expected, we retrieve similar trends for all analyzed cases, and all datasets converge towards a single branch in proximity of the theoretical prediction.

C. Communication Tests as a Function of Distance

As a final test, we analyzed the WLC performances of our OAs as a function of the distance between TX and RX, driving the WLED with constant nominal DC current and fixed modulation depth. Both signal amplitude and BER are recorded by varying the relative distance between light source and OAs (Fig. 5(a)–(b), respectively) in 5-cm steps, for all configurations discussed in previous sections (see the legend in Fig. 5(a)–(b). Error bars are not shown in order not to overload the figure and make it more readable. We neglect the errors on the positioning distance. Standard deviation on experimental amplitude values is ~ 0.2 mV, whilst BER error bars are obtained as the standard deviation on recorded data, and correspond to $\sim 4\%$. As our analysis is focused on comparing the performances of two OF-based OAs, we would like to point out that we are not targeting record distances, and low-power, off-the-shelf white LEDs have been used. Larger distances could be attained by selecting adequate higher-power LED in further developments.

First focusing on amplitude measurements (Fig. 5(a)), our results highlight that in [*White*] cases (hexagons), LR305 outperforms DQ1 for all distances. Moreover, above a distance of ~ 35 cm, using the LR305 OA grants larger signals as compared to the [*bare PD*] case. This indicates that the net OG of LR305 OA is larger than in that of bare PD, suggesting a clear advantage in employing LR305-based OAs in WLC systems. It should be

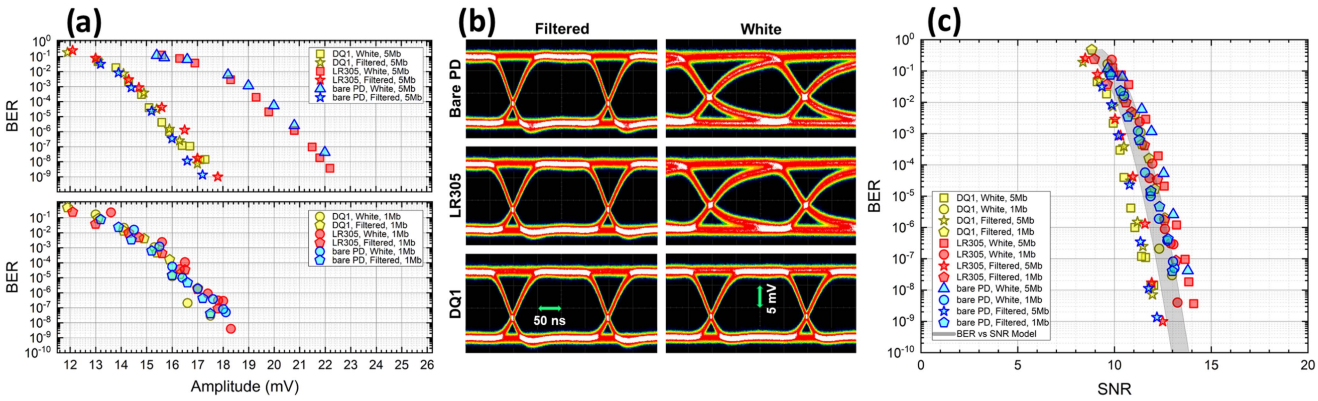

Fig. 4. Communication performance for both OAs, using WLED with and w/o blue filter as source: (a) recorded BER vs recorded signal amplitude, for 5 Mbps (upper panel) and 1 Mbps (lower panel); (b) eye diagrams for all RX configurations at 5 Mbps, for fixed signal amplitude (15 mV); (c) recorded BER vs recorded SNR (symbols) and model predictions (shaded area). The extension corresponds to the confidence interval of the model (see text).

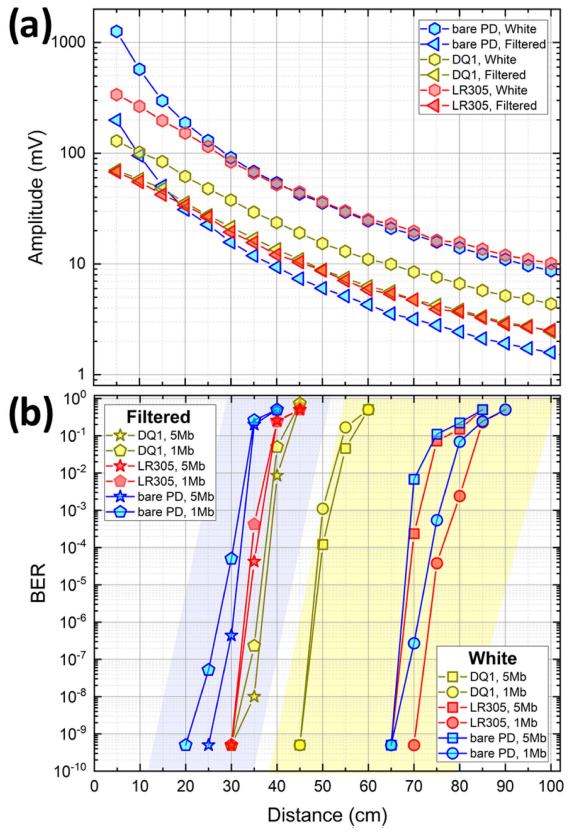

Fig. 5. (a) Signal amplitude recorded as a function of the distance between WLED and OAs. Two configurations are presented for the optical source ([*White*] and [*Filtered*], respectively). In addition to each OA configuration ([*DQ1*] and [*LR305*]) also [*bare PD*] configuration is analysed. (b) BER vs Distance between light source and OAs. The cluster of experimental data inside the blue area refers to [*Filtered*] configuration, whereas the yellow shaded area refers to [*White*] configuration, for both 1 Mbps and 5 Mbps rates.

also noted that the net OG could be further increased by either covering all the thin edges with PD elements, realizing larger FCs (depending upon the minimum BW to be achieved and on the strength of re-absorption effects), and/or coupling the PD with an index matching material (not employed in our setup).

In all cases, [*Filtered*] cases (triangles) feature globally lower signal strengths than [*White*] cases. In this, case both OAs more clearly outperform the [*bare PD, Filtered*] already above ~ 20 cm, with DQ1 featuring larger efficiencies than LR305 in the whole range. Therefore, our analysis suggests that DQ1 OAs are most effective in more specific blue/UV VLC applications.

In order to verify the indications obtained from pristine efficiency measurements, we show in Fig. 5(b) the BER values, measured as a function of distance, for all analyzed configurations, and for 1 Mbps and 5 Mbps rates (see legend for symbols assignment). Two clusters of data are highlighted by blue and yellow shaded areas, corresponding to [*Filtered*] and [*White*] scenarios, respectively. In our experimental conditions, data with BER $< 10^{-10}$ are considered as "error-free", and are not shown in the graph. Considering the [*Filtered*] scenario, where no BW limitations due to yellow LED phosphors lifetime are expected (see Section III-A), the communication performances are globally better when inserting OAs in the RX stage for both baud rates, and larger communication distances are attained as compared to the [*bare PD* cases] (blue/cyan symbols). This confirms that both our OA-based VLC systems benefit from the larger OG, with a slight out performance of DQ1 (yellow symbols) over LR305 (red symbols).

The [*White*] cluster data demonstrates that exploiting the whole white LED spectrum yields globally better performances in VLC applications with respect to the blue-filtered option, for a given WLED source, when no equalization techniques are involved [65], and larger system distances can be attained. It is evident that the most suited front-end for WLC applications is the LR305-based OA. At 1 Mbps, this device attains error-free distances of 0.70 m, outperforming the [*DQ1*] configuration, the latter featuring error-free distances of 0.45 m due to reduced conversion efficiency on yellow wavelength components (Section III-A). Noticeably, our analysis highlights equivalent or slightly superior LR305 OA performances as compared to [*bare PD*] setting, for both 1 Mbps and 5 Mbps rates. However, at 5 Mbps we notice that LR305 OA features slightly reduced link lengths as compared to the 1 Mbps case. As LR305 retains the WLED BW limitations, a reduced SNR and larger BW-induced

inter-symbol interference (ISI) are affecting the performance of the system. This effect is not visible in the case of DQ1 (yellow symbols) due to inherent self-blue-filtering effects of this OF (Section III-A).

Summarizing, our data show that in full white light applications the LR305 OA outperforms DQ1 OA, representing also a valid alternative to bare PD front-ends. We notice that larger OAs could be realized in future works, leveraging the advantages of LR305 further. Conversely, the self-blue filtering feature in DQ1 antenna eliminates BW limiting effects related to WLED sources also for higher data rates (5 Mbps) at the expense of its global efficiency for WLC applications, making the DQ1 antenna very promising for high-BW blue/UV light VLC applications. We would like to point out that the observed data rate is not limited by the intrinsic properties of the OAs, which are expected to support larger baud rates when fast TX optical sources are employed, or when pre/post equalization processes are put in play.

V. Conclusion

In our work, we realized and characterized two different OAs based on FC, for application in white light VLC. We employed two efficient fluorophores, originally developed for solar energy conversion, namely DQ1 and LR305. We characterized both intrinsic efficiencies of our OAs, such as the conversion efficiency using several LED sources with variable wavelength and the time response to external light stimuli, and their performances when integrated as an optical front end in a WLC communication system. Both OAs feature fast response times of the order of ~ 10 ns, comparable to the intrinsic lifetimes of the two OFs, making them suitable in large data rate applications. A Monte Carlo simulation has been furthermore implemented, demonstrating the ability to closely reproduce the experimental data on efficiency recorded as a function of the source wavelength. The employed theoretical model has a general validity and could be relevant in future developments of OAs for VLC and LSC applications. We validate our OAs in a complete WLC system, measuring SNR and BER as a function of distance between TX and RX for data rates up to 5 Mbps. Our tests are performed both with white- and blue-filtered light and show that LR305-based OAs represent an excellent alternative to conventional PD-based RX stages in WLC applications requiring few-MHz-BW, as, e.g., in many IoT applications. Conversely, in cases where blue/UV sources are employed, the best option is represented by DQ1 OAs, in view of their larger Stokes shift, reduced self-absorption [53] and better efficiency in the blue/UV range, suggesting that larger OAs could be realized as compared to LR305. The self-blue filtering property of DQ1 could be exploited to achieve large-BW WLC links, avoiding the slow yellow components typical of the WLEDs spectrum, at the expense of a reduced overall white light conversion efficiency. We highlight that a large margin for technical improvement exists for LR305 OAs, by, e.g., realizing larger slabs, equipping the uncovered portions of their edges with reflective coating, and using an index matching gel to couple the PD with the edge of the slab, which should boost their efficiency and communication performances even further. Our work represents a significant step towards full-fledged deployment of VLC using white light, where efficient, large-area and FoV, fast detectors with reduced angular dependence are key elements to exploit ordinary white LEDs as VLC transmitters. Moreover, as the presented OAs are based on efficient LSC fluorophores, efficiently converting white light, we envision that our results can be a reference for future works aimed at developing a new class of hybrid devices for joint WLC communication and solar energy harvesting, which could be efficiently integrated into smart buildings for the implementation of pervasive, energy-efficient networks.

Acknowledgment

The authors would like to thank all the members of VisiCoRe joint laboratory for useful discussions. They would also like to thank Mr. Massimo Ilarioni (I&S Srl, Rignano sull'Arno, Florence), Mr. Carlo Bartoli (ICCOM-CNR) and Mr. Andrea Donati (IFAC-CNR) for the support in the realization and polishing of the FCs.

References

[1] F. Guo, F. R. Yu, H. Zhang, X. Li, H. Ji, and V. C. M. Leung, "Enabling massive IoT toward 6G: A comprehensive survey," *IEEE Internet Things J.*, vol. 8, no. 15, pp. 11891–11915, Aug. 2021.

[2] N. Chen and M. Okada, "Toward 6G Internet of Things and the convergence with RoF system," *IEEE Internet Things J.*, vol. 8, no. 11, pp. 8719–8733, Jun. 2021.

[3] C. Yang et al., "Using 5G in smart cities: A systematic mapping study," *Intell. Syst. Appl.*, vol. 14, 2022, Art. no. 200065. [Online]. Available: https://www.sciencedirect.com/science/article/pii/S2667305322000060

[4] A. Gohar and G. Nencioni, "The role of 5G technologies in a smart city: The case for intelligent transportation system," *Sustainability*, vol. 13, no. 9, 2021, Art. no. 5188. [Online]. Available: https://www.mdpi.com/2071-1050/13/9/5188

[5] X. Qiao, P. Ren, G. Nan, L. Liu, S. Dustdar, and J. Chen, "Mobile web augmented reality in 5G and beyond: Challenges, opportunities, and future directions," *China Commun.*, vol. 16, no. 9, pp. 141–154, 2019.

[6] X. You et al., "Towards 6G wireless communication networks: Vision, enabling technologies, and new paradigm shifts," *Sci. China Inf. Sci.*, vol. 64, 2021, Art. no. 110301.

[7] M. Z. Chowdhury, M. Shahjalal, M. K. Hasan, and Y. M. Jang, "The role of optical wireless communication technologies in 5G/6G and IoT solutions: Prospects, directions, and challenges," *Appl. Sci.*, vol. 9, no. 20, 2019, Art. no. 4367. [Online]. Available: https://www.mdpi.com/2076-3417/9/20/4367

[8] L. E. M. Matheus, A. B. Vieira, L. F. M. Vieira, M. A. M. Vieira, and O. Gnawali, "Visible light communication: Concepts, applications and challenges," *IEEE Commun. Surv. Tuts.*, vol. 21, no. 4, pp. 3204–3237, fourthquarter 2019.

[9] D. Karunatilaka, F. Zafar, V. Kalavally, and R. Parthiban, "LED based indoor visible light communications: State of the art," *IEEE Commun. Surv. Tuts.*, vol. 17, no. 3, pp. 1649–1678, thirdquarter 2015.

[10] N. Chi, Y. Zhou, Y. Wei, and F. Hu, "Visible light communication in 6G: Advances, challenges, and prospects," *IEEE Veh. Technol. Mag.*, vol. 15, no. 4, pp. 93–102, Dec. 2020.

[11] W. Jiang, B. Han, M. A. Habibi, and H. D. Schotten, "The road towards 6G: A comprehensive survey," *IEEE Open J. Commun. Soc.*, vol. 2, pp. 334–366, 2021.

[12] D. Marabissi et al., "Experimental measurements of a joint 5G-VLC communication for future vehicular networks," *J. Sensor Actuator Netw.*, vol. 9, no. 3, 2020. [Online]. Available: https://www.mdpi.com/2224-2708/9/3/32

[13] M. Katz and I. Ahmed, "Opportunities and challenges for visible light communications in 6G," in *Proc. 2nd 6G Wireless Summit*, 2020, pp. 1–5.

[14] M. Figueiredo, C. Ribeiro, A. Dobesch, L. N. Alves, and O. Wilfert, "Consumer LED lamp with ODAC technology for high-speed visible light communications," *IEEE Trans. Consum. Electron.*, vol. 63, no. 3, pp. 285–290, Aug. 2017.

[15] A. Sewaiwar, P. P. Han, and Y. H. Chung, "3-Gbit/s indoor visible light communications using optical diversity schemes," *IEEE Photon. J.*, vol. 7, no. 6, pp. 1–9, Dec. 2015.

[16] R. Bian, I. Tavakkolnia, and H. Haas, "15.73 Gb/s visible light communication with off-the-shelf leds," *J. Lightw. Technol.*, vol. 37, no. 10, pp. 2418–2424, May 2019.

[17] H. Chun et al., "Visible light communication using a blue gan μ LED and fluorescent polymer color converter," *IEEE Photon. Technol. Lett.*, vol. 26, no. 20, pp. 2035–2038, Oct. 2014.

[18] S. Zhang et al., "A high-speed visible light communication system using pairs of micro-size LEDs," *IEEE Photon. Technol. Lett.*, vol. 33, no. 18, pp. 1026–1029, Sep. 2021.

[19] D. M. Maclure et al., "Gb/s optical wireless communications up to 17 meters using a UV-C micro-light-emitting diode," in *Proc. IEEE Photon. Conf.*, 2022, pp. 1–2.

[20] H. Haas, L. Yin, Y. Wang, and C. Chen, "What is LiFi?," *J. Lightw. Technol.*, vol. 34, no. 6, pp. 1533–1544, Mar. 2016.

[21] D. C. O'Brien, "Visible light communications: Challenges and potential," in *Proc. IEEE 24th Annu. Meeting Photonic Soc.*, 2011, pp. 365–366.

[22] S.-W. Wang et al., "A high-performance blue filter for a white-led-based visible light communication system," *IEEE Wireless Commun.*, vol. 22, no. 2, pp. 61–67, Apr. 2015.

[23] H. Le Minh et al., "High-speed visible light communications using multiple-resonant equalization," *IEEE Photon. Technol. Lett.*, vol. 20, no. 14, pp. 1243–1245, Jul. 2008.

[24] H. Le Minh et al., "100-Mb/s NRZ visible light communications using a postequalized white LED," *IEEE Photon. Technol. Lett.*, vol. 21, no. 15, pp. 1063–1065, Aug. 2009.

[25] A. M. Khalid, G. Cossu, R. Corsini, P. Choudhury, and E. Ciaramella, "1-Gb/s transmission over a phosphorescent white LED by using rate-adaptive discrete multitone modulation," *IEEE Photon. J.*, vol. 4, no. 5, pp. 1465–1473, Oct. 2012.

[26] M. A. S. Sejan and W.-Y. Chung, "Secure VLC for wide-area indoor IoT connectivity," *IEEE Internet Things J.*, vol. 10, no. 1, pp. 180–193, Jan. 2023.

[27] V. A. Reguera, L. Teixeira, C. H. Barriquello, D. H. Thomas, and M. A. Dalla Costa, "Efficient and low-complexity rate and dimming control of VLC for industrial IoT applications," *IEEE J. Emerg. Sel. Topics Ind. Electron.*, vol. 3, no. 4, pp. 1087–1095, Oct. 2022.

[28] J.-Y. Sung, C.-W. Chow, and C.-H. Yeh, "Is blue optical filter necessary in high speed phosphor-based white light led visible light communications?," *Opt. Exp.*, vol. 22, no. 17, pp. 20646–20651, Aug. 2014. [Online]. Available: https://opg.optica.org/oe/abstract.cfm?URI=oe-22-17-20646

[29] R. Mulyawan et al., "A comparative study of optical concentrators for visible light communications," in *Broadband Access Commun. Technol. XI*, ellingham, WA, USA: BInt. Soc. Opt. Photon., 2017, Art. no. 101280L, doi: 10.1117/12.2252355.

[30] M. Kong et al., "Toward self-powered and reliable visible light communication using amorphous silicon thin-film solar cells," *Opt. Exp.*, vol. 27, no. 24, pp. 34542–34551, Nov. 2019. [Online]. Available: https://opg.optica.org/oe/abstract.cfm?URI=oe-27-24-34542

[31] M. A. Khalighi and M. Uysal, "Survey on free space optical communication: A communication theory perspective," *IEEE Commun. Surv. Tuts.*, vol. 16, no. 4, pp. 2231–2258, Fourth Quarter 2014.

[32] P. P. Manousiadis et al., "Wide field-of-view fluorescent antenna for visible light communications beyond the étendue limit," *Optica*, vol. 3, no. 7, pp. 702–706, Jul. 2016. [Online]. Available: https://opg.optica.org/optica/abstract.cfm?URI=optica-3-7-702

[33] P. P. Manousiadis et al., "Optical antennas for wavelength division multiplexing in visible light communications beyond the Étendue limit," *Adv. Opt. Mater.*, vol. 8, no. 4, 2020, Art. no. 1901139. [Online]. Available: https://onlinelibrary.wiley.com/doi/abs/10.1002/adom.201901139

[34] M. Hammam, M. El-Mansy, S. El-Bashir, and M. El-Shaarawy, "Performance evaluation of thin-film solar concentrators for greenhouse applications," *Desalination*, vol. 209, no. 1, pp. 244–250, 2007. [Online]. Available: https://www.sciencedirect.com/science/article/pii/S0011916407001257

[35] S. Sadeghi et al., "Stokes-shift-engineered indium phosphide quantum dots for efficient luminescent solar concentrators," *ACS Appl. Mater. Interfaces*, vol. 10, no. 15, pp. 12975–12982, 2018, doi: 10.1021/acsami.7b19144.

[36] F. Meinardi et al., "Large-area luminescent solar concentrators based on 'stokes-shift-engineered' nanocrystals in a mass-polymerized pmma matrix," *Nature Photon.*, vol. 8, pp. 392–399, Apr. 2014. [Online]. Available: https://rdcu.be/daSP6

[37] S. Collins, "Smart phones: an example application for fluorescent concentrators," in *Proc. Glob. LIFI Congr.*, 2019, pp. 1–4.

[38] Y. Dong et al., "Nanopatterned luminescent concentrators for visible light communications," *Opt. Exp.*, vol. 25, no. 18, pp. 21926–21934, Sep. 2017. [Online]. Available: https://opg.optica.org/oe/abstract.cfm?URI=oe-25-18-21926

[39] M. A. Umair et al., "Long-range optical wireless communication system based on a large-area, Q-dots fluorescent antenna," *Laser Photon. Rev.*, vol. 17, no. 2, 2023, Art. no. 2200575. [Online]. Available: https://onlinelibrary.wiley.com/doi/abs/10.1002/lpor.202200575

[40] S. Collins, D. C. O'Brien, and A. Watt, "High gain, wide field of view concentrator for optical communications," *Opt. Lett.*, vol. 39, no. 7, pp. 1756–1759, Apr. 2014. [Online]. Available: https://opg.optica.org/ol/abstract.cfm?URI=ol-39-7-1756

[41] C. Quintana et al., "Ultra-wide coverage VLC system with alignment-free receiver," in *Proc. Glob. LIFI Congr.*, 2018, pp. 1–4.

[42] R. Mulyawan et al., "MIMO visible light communications using a wide field-of-view fluorescent concentrator," *IEEE Photon. Technol. Lett.*, vol. 29, no. 3, pp. 306–309, Feb. 2017.

[43] M. Sottile et al., "Epoxy resin doped with coumarin 6: Example of accessible luminescent collectors," *Eur. Polym. J.*, vol. 89, pp. 23–33, 2017. [Online]. Available: https://www.sciencedirect.com/science/article/pii/S0014305716317050

[44] D. A. Vithanage et al., "BODIPY star-shaped molecules as solid state colour converters for visible light communications," *Appl. Phys. Lett.*, vol. 109, no. 1, Jul. 2016, Art. no. 013302, doi: 10.1063/1.4953789.

[45] W. Ali, P. P. Manousiadis, D. C. O'Brien, G. A. Turnbull, I. D. W. Samuel, and S. Collins, "A Gigabit VLC receiver that incorporates a fluorescent antenna and a SiPM," *J. Lightw. Technol.*, vol. 40, no. 16, pp. 5369–5375, Aug. 2022.

[46] M. Portnoi et al., "Bandwidth limits of luminescent solar concentrators as detectors in free-space optical communication systems," *Light Sci. Appl.*, vol. 10, 2021, Art. no. 3.

[47] T. Peyronel, K. J. Quirk, S. C. Wang, and T. G. Tiecke, "Luminescent detector for free-space optical communication," *Optica*, vol. 3, no. 7, pp. 787–792, Jul. 2016. [Online]. Available: https://opg.optica.org/optica/abstract.cfm?URI=optica-3-7-787

[48] A. Riaz, G. Faulkner, and S. Collins, "A fluorescent antenna for white light visible light communications," in *Proc. Glob. LIFI Congr.*, 2019, pp. 1–4.

[49] C. He, Y. Lim, and H. Murata, "Study of using different colors of fluorescent fibers as optical antennas in white led based-visible light communications," *Opt. Exp.*, vol. 31, no. 3, pp. 4015–4028, Jan. 2023. [Online]. Available: https://opg.optica.org/oe/abstract.cfm?URI=oe-31-3-4015

[50] S. Chamani, A. Rostami, and P. Mirtaheri, "A superimposed QD-based optical antenna for VLC: White LED source," *Nanomaterials*, vol. 12, no. 15, 2022, Art. no. 2573. [Online]. Available: https://www.mdpi.com/2079-4991/12/15/2573

[51] J. Roncali, "Luminescent solar collectors: Quo vadis?," *Adv. Energy Mater.*, vol. 10, no. 36, 2020, Art. no. 2001907. [Online]. Available: https://onlinelibrary.wiley.com/doi/abs/10.1002/aenm.202001907

[52] G. Seybold and G. Wagenblast, "New perylene and violanthrone dyestuffs for fluorescent collectors," *Dyes Pigments*, vol. 11, no. 4, pp. 303–317, 1989. [Online]. Available: https://www.sciencedirect.com/science/article/pii/014372088985048X

[53] C. Papucci et al., "Luminescent solar concentrators with outstanding optical properties by employment of D–A–D quinoxaline fluorophores," *J. Mater. Chem. C*, vol. 9, pp. 15608–15621, 2021, doi: 10.1039/D1TC02923A.

[54] Z. Krumer, W. G. van Sark, R. E. Schropp, and C. de Mello Donegá, "Compensation of self-absorption losses in luminescent solar concentrators by increasing luminophore concentration," *Sol. Energy Mater. Sol. Cells*, vol. 167, pp. 133–139, 2017. [Online]. Available: https://www.sciencedirect.com/science/article/pii/S0927024817301745

[55] P. Della Sala et al., "First demonstration of the use of very large stokes shift cycloparaphenylenes as promising organic luminophores for transparent luminescent solar concentrators," *Chem. Commun.*, vol. 55, pp. 3160–3163, 2019, doi: 10.1039/C8CC09859J.

[56] A. P. Green and A. R. Buckley, "Solid state concentration quenching of organic fluorophores in PMMA," *Phys. Chem. Chem. Phys.*, vol. 17, pp. 1435–1440, 2015, doi: 10.1039/C4CP05244G.

[57] M. Seminara, T. Nawaz, S. Caputo, L. Mucchi, and J. Catani, "Characterization of field of view in visible light communication systems for intelligent transportation systems," *IEEE Photon. J.*, vol. 12, no. 4, pp. 1–16, Aug. 2020.

[58] C. Yang et al., "Consensus statement: Standardized reporting of power-producing luminescent solar concentrator performance," *Joule*, vol. 6, no. 1, pp. 8–15, 2022. [Online]. Available: https://www.sciencedirect.com/science/article/pii/S2542435121005730

[59] M. Bartolini et al., "Orange/red benzo[1,2-b:4,5-b']dithiophene 1,1,5,5-tetraoxide-based emitters for luminescent solar concentrators: Effect of structures on fluorescence properties and device performances," *ACS Appl. Energy Mater.*, vol. 6, no. 9, pp. 4862–4880, 2023, doi: 10.1021/acsaem.3c00362.

[60] "MathWorks(R) MATLAB version 9.13.0," (R2022b). [Online]. Available: https://mathworks.com/products/matlab.html

[61] D. Şahin, B. Ilan, and D. F. Kelley, "Monte-Carlo simulations of light propagation in luminescent solar concentrators based on semiconductor nanoparticles," *J. Appl. Phys.*, vol. 110, no. 3, Aug. 2011, Art. no. 033108, doi: 10.1063/1.3619809.

[62] S. Chamani, R. Dehgani, A. Rostami, H. Mirtagioglu, and P. Mirtaheri, "A proposal for optical antenna in VLC communication receiver system," *Photonics*, vol. 9, no. 4, 2022, Art. no. 241. [Online]. Available: https://www.mdpi.com/2304-6732/9/4/241

[63] S. Woei Leow, C. Corrado, M. Osborn, M. Isaacson, G. Alers, and S. A. Carter, "Analyzing luminescent solar concentrators with front-facing photovoltaic cells using weighted Monte Carlo ray tracing," *J. Appl. Phys.*, vol. 113, no. 21, Jun. 2013, Art. no. 214510, doi: 10.1063/1.4807413.

[64] H. Stern, S. Mahmoud, and L. Stern, *Communications Systems: Analysis and Design*. Hoboken, NJ, USA: Pearson Prentice Hall, 2004. [Online]. Available: https://books.google.it/books?id=-McoAAAACAAJ

[65] X. Huang, Z. Wang, J. Shi, Y. Wang, and N. Chi, "1.6 Gbit/s phosphorescent white led based VLC transmission using a cascaded pre-equalization circuit and a differential outputs pin receiver," *Opt. Exp.*, vol. 23, no. 17, pp. 22034–22042, Aug. 2015. [Online]. Available: https://opg.optica.org/oe/abstract.cfm?URI=oe-23-17-22034

Open Access funding provided by 'Università degli Studi di Firenze' within the CRUI CARE Agreement